Mechanical characterization of textile reinforced inorganic-matrix composites

T. D'Antino [a, b, *], Catherine Papanicolaou (Corina)[a]

[a] University of Patras, Department of Civil Engineering, GR-26500 Patras, Greece
[b] Politecnico di Milano, Department of Architecture, Built Environment, and Construction Engineering, IT-20133 Milan, Italy

This paper presents the results of the mechanical characterization of composite materials comprising high strength textiles embedded in inorganic matrices. These materials are commonly termed Textile Reinforced Mortars (TRM) or, when comprising cementitious matrices, Fabric-Reinforced Cementitious Matrix (FRCM – despite the fact that this term is often extended to composites with cement-free matrices). Different types of fibers were employed, namely carbon, glass, and basalt, as well as steel cords, which were embedded in lime- or cement-based matrices. Results of tensile tests on single fiber yarns and composite prismatic specimens with a rectangular cross-section are shown and discussed. The effect of fiber coating and stitch-bonded joints between warp and weft yarns on the tensile behavior observed is studied. The results obtained help to shed light on the different parameters that affect tensile testing of inorganic-matrix composites contributing to the appropriate mechanical characterization of these materials.

Keywords:
Inorganic matrix
FRCM
TRM
Tensile tests

1. Introduction

Fiber reinforced composites represent a viable solution for strengthening and retrofitting existing structural elements. Among them, Fiber Reinforced Polymer (FRP) composites have gained great popularity in the last decades due to their ease of installation, high strength-to-weight ratio, and relatively limited curing time [1]. However, the use of organic binders in FRP composites is respon-sible for some drawbacks, such as poor performance to relatively high temperatures, poor compatibility with substrates such as masonry, vapor barrier formation, and difficulties in application onto wet surfaces. In order to overcome these issues, organic binders (in combination with continuous fiber sheets) were substituted with inorganic ones (in combination with fiber grids) to form a new generation of high strength composite materials with resistance to high temperatures [2–4] and improved compatibility with concrete and masonry substrates [5–7]. Different names have been proposed to describe these inorganic-matrix fiber reinforced composite materials: Textile Reinforced Concrete (TRC) is a term used to describe composite materials, which were originally meant to be integrated in new civil applications rather than used as strengthening means for existing structures, comprising thin layers of (fine-grained) concrete (basically a high strength mortar) reinforced with high strength textiles (i.e. fiber grids) [8–10] – in this case, the term aims at stressing the structural character of the new material in an effort to increase market awareness and acceptance; the term Textile Reinforced Mortar (TRM) describes essentially the same type of inorganic-matrix composites with a primary field of application in the strengthening/retrofitting of existing structures following the wet lay-up method [11]; the term Fabric- (as per ACI 549.4R-13 [12]) or Fiber- (as per other authors [5,13,14]) Reinforced Cementitious Matrix (FRCM) describes composite materials consisting of a sequence of one or more layers of cement-based matrix reinforced with dry fibers in the form of open single- or multiple-layer meshes [15–17]; the term Steel Reinforced Grout (SRG) de-scribes composite materials comprising steel cords formed by interwoven steel wires embedded in a cementitious grout matrix [18]. In this paper, the acronym TRM is used as a general term to indicate textile reinforced composites with either lime- or cement-based matrices.

Although TRM composites have already been used to strengthen existing structures for more than a decade [19] homogenized/normalized testing methods and design procedures are still lacking in Europe. In the U.S., FRCM tensile properties are recommended

* Corresponding author. University of Patras, Department of Civil Engineering, GR-26500 Patras, Greece.
E-mail address: tommaso.dantino@polimi.it (T. D'Antino).

Published Journal Article available at: http://dx.doi.org/10.1016/j.compositesb.2017.02.034

(by ACI 549.4R-13 [12]) to be determined according to the test procedure specified in Annex A of AC434-13 [20]. This document provides guidelines for the necessary tests and calculations required for any FRCM system to receive a product research report from the International Code Council Evaluation Service (ICC-ES); such a report can then be used as a supporting document for certifying building code compliance according to the International Building Code (IBC 2012 [21]). The drafting of appropriate testing methods for textile reinforced inorganic-matrix composites has also been the subject of Rilem activities. The Rilem Technical Committee 234-DUC (Design procedures for the use of composites in strengthening of reinforced concrete structures) presented a procedure for the mechanical characterization of inorganic-matrix composites through tensile and bond tests [22]. Recently, the Rilem Technical Committee 232-TDT (Test methods and design of textile reinforced concrete) published a recommendation regarding the uniaxial tensile test of TRC coupons [23]. Additionally, the Rilem Technical Committee 250-CSM (Composites for the sustainable strengthening of masonry) organized (during 2014–2015) a Round Robin Test (RRT) campaign to experimentally investigate the tensile and bond behavior of different inorganic-matrix composites [24–28].

Tensile tests on inorganic-matrix composite material samples are an integral part of the mechanical characterization thereof and are used both for classifying/comparing different matrix/textile combinations (market products) and for providing useful design values to engineers. The mechanical properties obtained from separate tests on fibers and matrix cannot be directly employed to obtain the mechanical properties of the composite material [29]. This is owed to the interaction between the brittle (and multi-phase) matrix with the open-weaved fabric (textile). This interaction results in multiple cracking of the matrix and – for most cases – in relative slip between the fibers and the matrix. The specifics of the tensile test procedure for this type of composites play a decisive role in capturing their characteristic axial stress-strain behavior. The term "characteristic" is used here to describe the in-service representative behavior of the inorganic-matrix composite materials under direct tension (predominantly parallel to the principal fiber direction). It should be pointed out, however, that the tensile test cannot always accurately reflect the in-service tensile loading/boundary conditions [30].

Different set-ups for tensile testing of composite materials comprising fiber textiles and inorganic matrices have been proposed in the literature. Set-ups mainly differ in specimen morphology, clamping method, and measurement technique. The most commonly used specimen types are the rectangular prism [8,9,16,31] and the dumbbell [29,32–34], with or without increasing the thickness or the width of the specimen at the ends. Clamping methods for rectangular prisms include direct clamping by hydraulic or pneumatic wedges (referred to as *clamping grip*) [16], clamping of specimen ends by through-bolted steel plates connected to the machine by hinge joints [9,35], bonding of steel or aluminum plates to the specimen ends and connecting the plates to the machine through hinge joints (referred to as *clevis grip*) [17,36], and drilling of holes in the specimen ends and clamping of the steel rods inserted through the holes [31,37] – this technique is also applicable to dumbbell specimens, see Ref. [29]. Dumbbell specimens are usually secured at the machine heads using self-adjustable curved steel flanges matching the radius of the load introduction zone of the specimen and equipped with (at least) a rotational capacity in its plane; steel flanges are padded with rubber sheets in order to avoid stress concentrations between steel and mortar. During testing the axial deformation can be measured by either Linear Variable Differential Transformers (LVDTs) or exten-someters applied on the specimen, by digital image correlation (DIC) techniques, or by using the stroke of the machine [18].

Each test set-up described can be associated with a different control mode. Although tensile tests on TRC specimens were conducted under force control [38], tensile tests on inorganic-matrix composites are generally carried out in displacement control by increasing the stroke of the machine. Displacement rates adopted in the literature vary between 0.0017 mm/s [33] and 0.017 mm/s [10,29,31], with intermediate values of approximately 0.0084 mm/s [18,36]. A displacement rate not constant along the entire test but increased from 0.0017 mm/s to 0.0084 mm/s after the occurrence of the first cracks [16] was also reported in the literature. It should be noted that the control mode and rate adopted may have a strong influence on the results. Evidence from single-lap direct-shear tests conducted on inorganic-matrix composites comprising PBO fibers bonded to concrete blocks showed that the control mode (machine stroke or external LVDT) and the displacement rate have a strong influence on the load response obtained [39]. Studies available in the literature do not provide a clear understanding of the influence of the rate adopted. Further investigations are needed to provide reliable indications regarding the control mode for tensile testing of inorganic-matrix composites.

Each test set-up proposed presents some drawbacks, and results obtained by different set-ups cannot be easily compared. Tests carried out on rectangular prism specimens with two different clamping methods showed that the results obtained were highly dependent upon the set-up adopted [9]. In general, results of tensile tests on inorganic-matrix composite materials are affected by the presence of in-plane and out-of-plane bending moments, fabrication defects, and measurement technique employed [31]. Furthermore, several parameters, such as the textile geometry and manufacturing process, cross-sectional shape of bundles, presence of stich-bonded joints between longitudinal and transversal bundles, and coating or impregnation of textiles, affect the behavior of the composite material and need to be properly investigated.

Failure of TRM composites applied as strengthening of existing structures may occur due to debonding of the fiber from the embedding matrix, interlaminar (delamination [40]) failure, detachment of the composite strip from the substrate (without damage of the substrate itself), or by debonding within a thin layer of substrate [14,22]. The failure mode of TRM composites comprising one or two layers of textile is generally reported to be debonding of the fiber from the embedding matrix [5,16], whereas detachment of the composite strip, interlaminar failure, and debonding within the substrate were observed when 3 or 4 layers of textile are employed [40,41]. The mechanical characterization of TRM composites should be conducted on specimens comprising one layer of textile and, if expected by the specific application, multiple-layers tests should be also carried out [20]. However, since employing more than two layers of textile would shift the failure mode to the matrix-substrate interface of within the substrate, bond tests rather than tensile tests should be performed to study the behavior of such multiple-layers composites.

This paper shows the results obtained from six different TRM composites subjected to tensile loading using rectangular prism specimens. TRM composites studied include one layer of carbon, glass, basalt, or steel textile combined with lime- or cement-based mortar. Some of the tests performed were part of the RRT campaign promoted within the framework of Rilem TC 250-CSM. Although further investigations are needed to understand the load response of the same composite materials for different numbers of textile layers, the results obtained help to shed light on the different parameters that affect tensile testing of TRM composites contributing to the appropriate mechanical characterization of these materials.

2. Idealized stress-strain response

Although TRM composites comprising different textiles and matrices may present different tensile behaviors, an idealized trilinear stress-strain response, reported with a dashed line in Fig. 1a, was proposed for this type of inorganic-matrix composites [38,42,43]. The response of the corresponding real specimen is also reported in Fig. 1a with a continuous line for comparison.

The idealized trilinear stress-strain response should be independent of the test set-up adopted for the tensile test. However, in reality, the specimen morphology, fiber volume fraction in the longitudinal direction, clamping method, and control mode may affect the response, as discussed below. It should be noted that, although it may play an important role (see Section 1), the influence of the control mode on the stress-strain response is not discussed in this work.

According to the idealized stress-strain response of Fig. 1a, the material responds in a linear elastic manner while uncracked. This stage, named Stage 1 or uncracked stage, ends with the occurrence of the first crack in the matrix, which is sometimes responsible for a sudden drop in the applied stress. With increasing deformation, further cracks appear along the specimen length and the axial stress does not increase significantly (Stage 2 or crack development stage). When the matrix is unable to form additional cracks (i.e. when matrix crack saturation is achieved) the applied load is sustained solely by the longitudinal (load-aligned) fibers (Stage 3 or post-cracking stage). Therefore, Stage 3 should be characterized by a slope of the stress-strain curve similar to the elastic modulus of the bare (matrix-free) fibers and failure should occur due to fiber rupture.

However, rupture of some filaments may occur during Stage 2 leading to a decrease of the axial stiffness of the composite material at Stage 3 with respect to the theoretical value based on the axial stiffness of the bare fibers. Additionally, depending on the test set-up adopted and on the characteristics of the composite material, fibers may slip within the matrix throughout Stages 2&3. In this case, fiber rupture may not occur (or occur only for those fiber filaments "impregnated" by the matrix [44]) and Stage 3 would be characterized by fiber slippage. For some composites characterized by (relatively) low-strength matrix and slippage of the fibers, Stage 2 cannot be distinguished from Stage 3 [17]. It should be noted that absence of Stage 2 was also observed for cementitious composite materials with high-strength matrix, high fiber volume fractions and good matrix-fiber bond capacity [45]. The stress-strain response of these types of composite can be idealized with a bilinear behavior, as shown by the dashed line in Fig. 1b. The response of the corresponding real specimen is also reported in Fig. 1b with a continuous line for comparison.

In order to prevent fiber slippage and attain fiber rupture at the end of tensile tests, the clamping grip method was employed [16,46]. The clamping grip method, which induces pressure to the specimen ends improving the stress-transfer mechanism between fibers and matrix and preventing fiber slippage, allows for the full exploitation of the fibers along the loading direction and, hence, for obtaining the ultimate load-bearing capacity of the composite under tension. However, the use of clamping grips induces stress concentration to the specimen ends that could lead to failure (crushing) of the matrix inside the clamping area or premature failure of the specimen just outside the clamping area [35]. Although different techniques were proposed to strengthen the specimen ends against premature failure induced by the clamping grip method (e.g. bonded FRP tabs, FRP wrappings, rubber pads [25]) in order to avoid failure of the matrix close or within the clamping area, this detailing still remains a difficult task. Moreover, clamping of the specimen ends corresponds to end conditions that are not likely to be present in real-life applications unless the composites are expected to be fixed onto the substrate by use of mechanical anchoring systems that will exert a compressive stress normal to the plane of the composite. Therefore, parameters obtained with the clamping grip method should be employed for characterizing the composite material but should not be directly used as input parameters for design purposes.

In general, maximum attainable strength of inorganic-matrix composites can be achieved employing the clamping grip method (preferably with a bilateral global rotational capacity) provided that: i) a defect-free specimen is used (defects being, for example, preexisting cracks, warping, and unsymmetrical textile position with respect to the specimen thickness) and ii) the clamping stress does not cause premature cracking within the clamping areas and/or adjacent to them.

According to the idealized trilinear response depicted in Fig. 1a, the tensile stress-strain curves of TRM specimens can be defined by 9 parameters, namely stresses σ_1, σ_2, and σ_u, the corresponding strains ε_1, ε_2, and ε_u, respectively, and the slopes E_1,E_2, and E_3 of the three branches comprising the trilinear response. The stress σ_1 and the corresponding strain ε_1 define the point of transition between Stage 1 and Stage 2, which coincides with the occurrence of the first matrix crack. The stress σ_2 and the corresponding strain ε_2 define

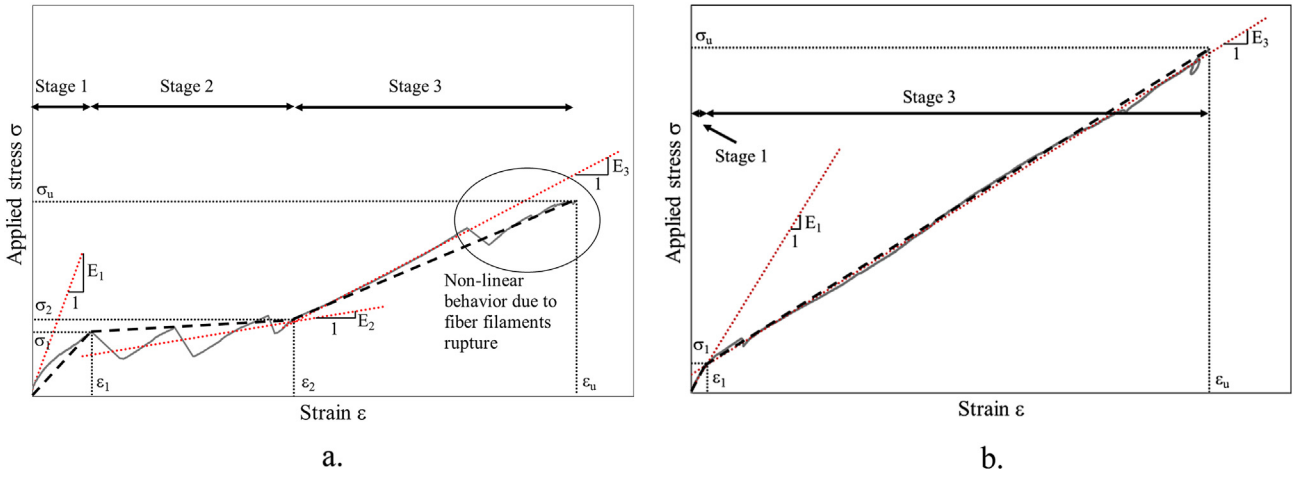

Fig. 1. Identification of different response Stages according to the idealized (dashed lines) trilinear stress-strain response of specimens with (a) and without (b) the presence of Stage 2.

the point of transition between Stage 2 and Stage 3, which corresponds to the onset of the linear branch of the stress-strain curve where the applied load is carried only by the fibers. Failure of the specimen is indicated by the ultimate stress σ_u and corresponding strain ε_u. Stresses can be computed based both on the specimen gross cross-section and on the cross-sectional area of the longitudinal fibers.

Stages 1, 2, and 3 are characterized by slopes E_1, E_2, and E_3, respectively. Since the determination of the 9 parameters is not always straightforward, a procedure that also involves fitting of the stress-strain curve is employed in this work. Due to the non-linear behavior of the stress-strain curve, the slopes corresponding to the different stages may be different from the slope of the lines that connect points of transition and that identify the trilinear or bilinear response (dashed lines in Fig. 1a and b, respectively). Indeed, for some TRM composites Stage 1 presents a linear branch followed by a non-linear response up to the onset of the first crack (Fig. 1a). This non-linear response is ought to gradual micro-cracking of the matrix resulting in the first macro-crack (the through-crack denoting the onset of Stage 2). In this case, E_1 is evaluated as the slope of the linear branch of Stage 1 (dotted line in Fig. 1). The slope of the crack development stage (Stage 2) is evaluated by fitting the stress-strain curve between points (σ_1, ε_1) and (σ_2, ε_2), which in general provides a slope different from that corresponding to the line connecting points (σ_1, ε_1) and (σ_2, ε_2)(Fig. 1a). When the first matrix crack is not clearly recognizable, ε_1 is computed as the strain corresponding to the point of intersection between lines with slope E_1 and E_2 (or E_3 in the case where Stage 2 is not present - see Fig. 1b). In this case, E_2 (or E_3) is evaluated by fitting the stress-strain curve along the assumed Stage 2 (or Stage 3), which would be characterized by a slope significantly lower than that of Stage 1.

For some TRM composites, progressive rupture of fiber filaments during Stage 3 may lead to a non-linear behavior of the stress-strain curve before rupture of the textile occurs (Fig. 1a). In these cases, slope E_3 is evaluated as the slope of the linear branch of Stage 3 (see the dotted line in Fig. 1a).

3. Experimental program

3.1. Materials

Six different TRM composites including a single layer of textile embedded within inorganic matrices were tested. The TRM composites studied included carbon fibers with and without coating, coated basalt fibers, coated glass fibers, and galvanized steel cords. It should be noted that all coated textiles tested in this study were fully impregnated by the resin. Although using the term “impregnated textile/yarn” would be more appropriate, the term “coated” is used hereafter in line with the existing literature and market practice. The fiber textiles employed, which are shown in Fig. 2, were named following the notation FKC, where F = fiber employed (C = carbon, B = basalt, G = glass, S = steel), K = area weight of the textile employed in g/m^2, and C (if present) = presence of coating. Fiber textiles with different area weight, coating (where present), grid spacing, and presence of stitches between longitudinal and transversal rovings were used:

- Textile C170C (Fig. 2a) comprised a balanced bidirectional grid consisting of coated carbon fiber rovings spaced at 20 mm in both directions, with an area weight (without coating) of 170 g/m^2;
- Textile C170 (Fig. 2b) was identical to textile C170C, but without coating. Although the cross-sectional area of each roving was equal for textiles C170 and C170C, the shape of the cross-section was different (Fig. 2a and b).
- Stitch-bonded textile C220C (Fig. 2c) comprised a balanced bidirectional grid consisting of coated carbon fiber rovings spaced at 30 mm in both directions, with an area weight (without coating) of 220 g/m^2. Rovings were impregnated with a high temperature resistive coating and connected through stitches. Stitches are responsible for the wavy shape of the warp rovings, whereas the weft rovings remained plane.
- Stitch-bonded textile B170C (Fig. 2d) comprised a balanced bidirectional grid consisting of basalt fiber rovings spaced at 25 mm in both directions, with an area weight (without coating) of 170 g/m^2. Rovings were impregnated with a high temperature resistive coating and connected through stitches. Stitches are responsible of the wavy shape of the warp rovings, whereas the weft rovings remained plane.
- Textile G250C (Fig. 2e) comprised a balanced bidirectional grid consisting of coated AR glass fiber rovings spaced at 25 mm in both directions, with an area weight (without coating) of 250 g/m^2.
- Textile S80 (Fig. 2f) was made of unidirectional galvanized steel cords spaced at 7.5 mm, each comprising 5 wires (2 wires twisted around 3 rectilinear wires), with an area weight of 80 g/m^2.

The mechanical properties of the textiles used were investigated by tensile tests on single fiber rovings taken from the warp direction. Specimens comprised one fiber roving 500 mm long. FRP tabs were epoxy-bonded to the ends of the specimen to ensure slip-free gripping by the testing machine. The cross-sectional area of the single roving A_f (Table 1) was computed from the nominal thickness provided by the manufacturers. Tests were conducted in displacement-control at a rate of 0.5 mm/min following ASTM D3039 [47]. A clip-on extensometer was applied to the center of each specimen to measure the strain of the roving. The mean tensile strength σ_f, the corresponding mean strain ε_f, and the mean elastic modulus E_f were obtained by averaging the results of at least 3 specimens for each textile and are reported in Table 1 together with the

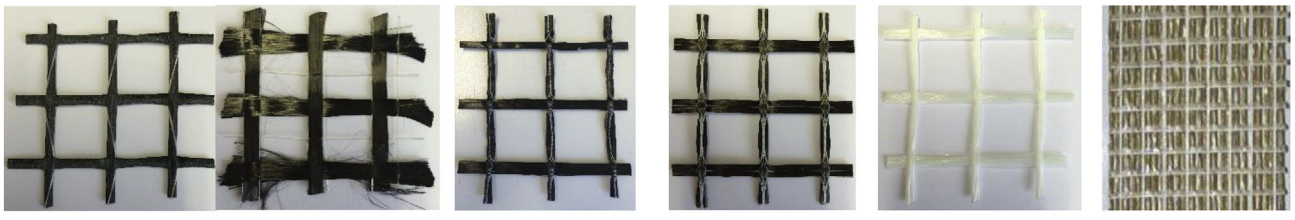

Fig. 2. Textiles employed: a) Coated carbon C170C; b) Carbon C170; c) Stitch-bonded coated carbon C220C; d) Stitch-bonded coated basalt B170C; e) Coated glass G250C; f) Galvanized steel S80. Note: warp rovings are displayed in vertical direction.

Table 1
Properties of textiles employed (warp direction).

Textile	Area weight [g/m^2]	Coating	Spacing [mm]	A_f [mm^2]	σ_f [MPa] (CoV)	ε_f [%] (CoV)	E_f [MPa] (CoV)
C170C	170	✓	20	0.94	1890 (0.132)	0.94 (0.033)	219000 (0.048)
C170	170	×	20	0.94	938 (0.093)	1.80[a]	240000[a]
C220C	220	✓	30	1.89	1800 (0.087)	0.86 (0.027)	227000 (0.133)
G250C	250	✓	25	1.25	660 (0.126)	1.41 (0.020)	55000 (0.220)
B170C	170	✓	25	0.83	1900 (0.050)	1.86 (0.086)	107000 (0.118)
S80	80	×	7.5	0.54	3350 (0.051)	2.25 (0.092)	185000 (0.100)

[a] Provided by the manufacturer.

corresponding coefficient of variation, CoV. Values of ε_f and E_f obtained for textile C170 were disregarded because the clip-on extensometer was not firmly attached onto the specimens due to the absence of coating. Values of ε_f and E_f declared by the manufacturer are reported in Table 1 for textile C170. With the exception of a single value (E_f of textile G250C) good repeatability of results was achieved (CoVs lower than 13.5%).

Three different matrices used in combination with a specific type of fiber textile (to produce a specific market product as indicated by the different manufacturers) were employed:

- Matrix C is a thixotropic fiber-reinforced cement-based mortar;
- Matrix L is a lime-based mortar with silica sand;
- Matrix P is a lime-based mortar with pozzolanic binders, synthetic fibers, and graded sand with a diameter lower than 3 mm.

Each matrix employed was mechanically characterized. A minimum of three 40 mm × 40 mm × 160 mm prisms were cast from each batch of matrix used to prepare the TRM specimens and were tested according to EN 1015-11 [48]. Ten batches were cast at different times for specimens with matrix C, 3 batches for specimens with matrix L, and 1 batch for specimens with matrix P. The average flexural strength $\sigma_{m,f}$ and average compressive strength σ_c obtained from each matrix batch are reported in Table 2 together with the corresponding coefficient of variation, CoV (lower than 17% for all cases).

3.2. Specimens and test set-up

All TRM composites were tested using rectangular prism specimens with nominal length and thickness equal to 500 mm and 10 mm, respectively (Fig. 3a). The specimens were cut from a plate with dimensions 500 mm × 375 mm cast using a steel formwork to control the thickness of the matrix and the position of the fiber textile. Prior to testing, the planarity of each specimen was checked and curved (slightly bowed) specimens were disregarded. Nevertheless, due to difficulties in properly tensioning each bundle during casting, which caused out-of-plane misalignment of (relatively) loose bundles during mortar pouring, the textile was slightly offset from the mid-thickness plane in some specimens. This offset was more pronounced for specimens incorporating carbon C220C and basalt B170C textiles due to the presence of the fiber coating and stitch-bonded joints that made these textiles stiff and difficult to manage. The width of the specimens b_1 (Fig. 3a) was varied, depending on the textile employed, to include at least 3 longitudinal bundles and to be a multiple of the bundle spacing. Specimens were cured under laboratory conditions (23 °C and 60% RH, approximately) for at least 28 days before testing.

All specimens were strengthened using FRP sheets wrapped around their ends. Two layers of carbon FRP sheets with a nominal thickness of 0.22 mm per layer were wrapped around each end for a length of 80 mm. The strengthened ends of the rectangular prism specimens were clamped directly by the machine hydraulic wedges (clamping grip method), which had a length of 80 mm and applied a clamping force orthogonal to the specimen surface of approxi-mately 76 kN. This clamping force resulted in a clamping stress σ_w of approximately 15.80 MPa for specimens with textiles C170C and C170, 10.60 MPa for specimens with textile C220C, 12.70 MPa for specimens with textiles G250C and B170C, and 21.10 MPa for specimens with textiles S80. The clamping force was selected to provide a clamping stress close to the compressive strength of the matrix employed except for composites with textile S80 where the clamping stress applied was increased with respect to the corresponding matrix strength in an attempt to avoid fiber slippage (see Section 4.3). However, FRP wrapping of specimens ends is expected to increase the compressive strength of the matrix and, therefore, it should prevent compressive failure in the gripping area. Tests were conducted by controlling the stroke of the machine, which was increased at a constant rate of 0.004 mm/s. The longitudinal strain was measured using 2 LVDTs with a stroke of 5 mm applied on each side of the specimen. The LVDTs were mounted on steel supports spanning over a length of 210 mm (Fig. 3a). The set-up employed in this work (Fig. 3b) constrained all rotational degrees of freedom at the specimens ends.

Specimens (as listed in Table 3) were named following the notation R_MT_X_Y_Z, where R = rectangular prism specimen; M = matrix employed (C, L, or P); T = textile employed (according to the nomenclature explained above); X = specimen overall length (in mm); Y = width of the specimen b_1 (in mm); Z = specimen number. A minimum of 3 specimens was tested for each composite material. The number of specimens tested varied from a minimum of 3 to a maximum of 10 (see Table 3) depending on the scatter obtained in the results and on the dimension of the specimens themselves, which were all cast using a plate with dimensions 500 mm × 375 mm (see Section 3.2).

All stress values in Table 3 (except $\sigma_{1,m}$) have been obtained by dividing the applied load by the textile area $n \cdot A_f$, where n is the number of longitudinal yarns included in the specimen. The stress corresponding to the onset of matrix cracking was also computed by dividing the applied load by the nominal gross cross-sectional

Table 2
Mechanical properties of the matrices employed.

Matrix name	Matrix type	$\sigma_{m,f}$ [MPa] (CoV)	σ_c [MPa] (CoV)
C	Cement-based	6.70 (0.145)	16.40 (0.169)
L	Lime-based	6.10 (0.132)	12.10 (0.075)
P	Lime-based + pozzolanic binders	5.00 (0.099)	10.30 (0.064)

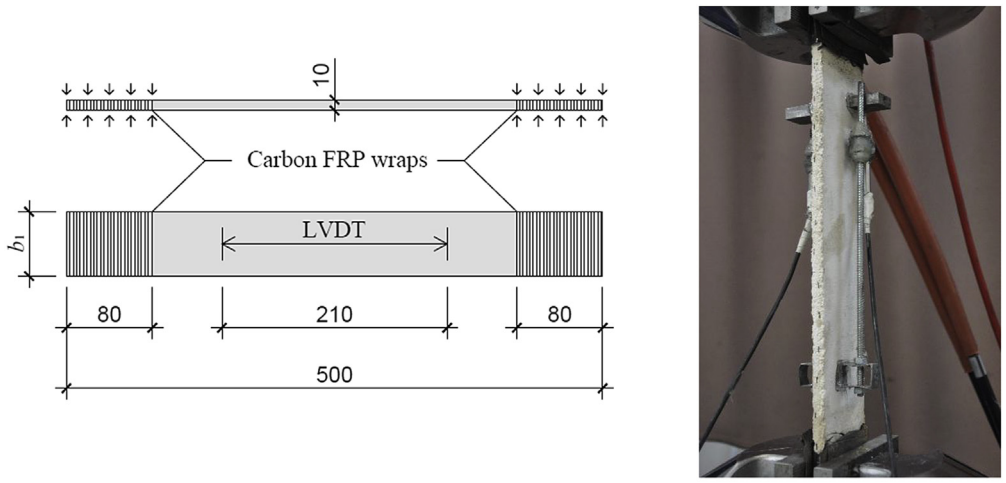

Fig. 3. a) Geometry of rectangular prism specimens (dimensions in mm). b) Photo of the test set-up (specimen R_PB170C_500_75_1).

Table 3
Results of tensile tests on rectangular prism specimens.

Rectangular prism	n	σ_1 [MPa]	ε_1 [%]	E_1 [GPa]	σ_2 [MPa]	ε_2 [%]	E_2 [GPa]	σ_u [MPa]	ε_u [%]	E_3 [GPa]	$\sigma_{1,m}$ [MPa]	FM
R_CC170C_500_60_1	3	2520	0.08	3220	2572	0.60	44	2840	0.87	166	11.80	C
R_CC170C_500_60_2	3	1650	0.05	3450	2374	0.63	76	2900	0.92	230	7.80	C
R_CC170C_500_60_3	3	1500	0.04	3780	2365	0.54	86	2940	0.87	177	7.10	C
R_CC170C_500_60_4	3	1950	0.07	3290	2194	0.56	74	2880	0.89	229	9.20	C
R_CC170C_500_60_5	3	1000	0.03	3390	–	–	–	2600	0.51	179	4.70	C
R_CC170C_500_60_6	3	1252	0.04	2935	1915	0.80	59	2310	1.07	147	5.90	A
Avg		1645	0.05	3344	2284	0.63	68	2745	0.86	188	7.70	–
CoV		0.327	0.376	0.083	0.108	0.165	0.242	0.089	0.216	0.181	0.327	–
R_CC170C_500_60_7	3	411	0.12	873	489	0.52	53	1250	1.08	171	1.90	A
R_CC170C_500_60_8	3	512	0.15	371	673	0.41	104	1430	0.76	208	2.40	C
R_CC170C_500_60_9	3	431	0.20	274	464	0.36	55	1400	0.83	200	2.00	C
R_CC170C_500_60_10	3	442	0.12	510	562	0.54	59	1320	0.96	205	2.10	C
Avg		449	0.15	507	547	0.46	68	1350	0.91	196	2.10	–
CoV		0.098	0.256	0.518	0.171	0.189	0.359	0.060	0.156	0.087	0.098	–
R_CC170_500_60_1	3	177	0.03	454	–	–	–	794	0.65	129	0.80	C
R_CC170_500_60_2	3	132	0.03	341	–	–	–	870	0.77	98	0.60	C
R_CC170_500_60_3	3	379	0.07	1215	–	–	–	851	0.78	–	1.80	C
Avg		229	0.04	670	–	–	–	838	0.73	114	1.10	–
CoV		0.574	0.533	0.709	–	–	–	0.047	0.099	0.193	0.574	–
R_PC220C_500_90_1	3	125	0.31	24	174	0.95	21	1031	1.88	370	0.80	C
R_PC220C_500_90_2	3	94	0.04	15	301	1.19	15	1062	1.70	200	0.60	C
R_PC220C_500_90_3	3	84	0.02	366	301	1.85	12	1060	2.31	280	0.50	C
R_PC220C_500_90_4	3	65	0.04	120	355	1.21	20	1020	2.02	130	0.40	C
Avg		92	0.10	131	283	1.30	17	1043	1.98	245	0.60	–
CoV		0.273	1.353	1.246	0.272	0.296	0.250	0.020	0.130	0.422	0.273	–
R_PB170C_500_75_1	3	357	0.03	2014	441	0.32	37	1397	2.10	166	1.20	A
R_PB170C_500_75_2	3	272	0.04	1343	450	0.77	17	1076	1.78	107	0.90	A
R_PB170C_500_75_3	3	245	0.09	439	523	1.01	28	1339	1.80	126	0.80	A
R_PB170C_500_75_4	3	261	0.17	337	661	1.37	29	1292	2.40	67	0.90	B
R_PB170C_500_75_5	3	375	0.14	978	388	0.60	20	1291	2.04	168	1.20	A
Avg		302	0.09	1022	493	0.81	26	1279	2.02	127	1.00	–
CoV		0.197	0.647	0.674	0.215	0.491	0.302	0.095	0.125	0.335	0.197	–
R_LG250C_500_75_1	3	1020	0.06	1940	–	–	–	1220	0.89	63	5.10	B
R_LG250C_500_75_2	3	800	0.07	1480	974	0.53	28	1510	1.74	44	4.00	B
R_LG250C_500_75_3	3	690	0.05	1290	659	0.44	2	1360	2.20	38	3.50	B
R_LG250C_500_75_4	3	780	0.07	1490	800	0.29	26	1450	1.96	33	3.90	B
R_LG250C_500_75_5	3	850	0.05	1540	804	0.29	6	1410	1.21	70	4.30	B
R_LG250C_500_75_6	3	456	0.05	1087	546	0.34	21	785	0.93	54	2.30	B
R_LG250C_500_75_7	3	642	0.06	1110	693	0.38	29	1107	1.23	57	3.20	B
R_LG250C_500_75_8	3	808	0.06	1599	–	–	–	1196	0.83	78	4.00	B
R_LG250C_500_75_9	3	448	0.06	1056	–	–	–	950	1.46	36	2.20	B
Avg		722	0.06	1399	746	0.38	19	1221	1.38	53	3.60	–
CoV		0.257	0.134	0.208	0.198	0.247	0.630	0.198	0.356	0.303	0.257	–
R_CS80_500_45_1	6	177	0.03	522	–	–	–	2214	1.04	200	1.30	C
R_CS80_500_45_2	6	277	0.03	1152	–	–	–	1622	0.72	207	2.00	C
R_CS80_500_45_3	6	97	0.01	531	–	–	–	1561	0.94	149	0.70	C
Avg		184	0.02	735	–	–	–	1799	0.90	185	1.30	–
CoV		0.491	0.495	0.491	–	–	–	0.200	0.181	0.171	0.491	–

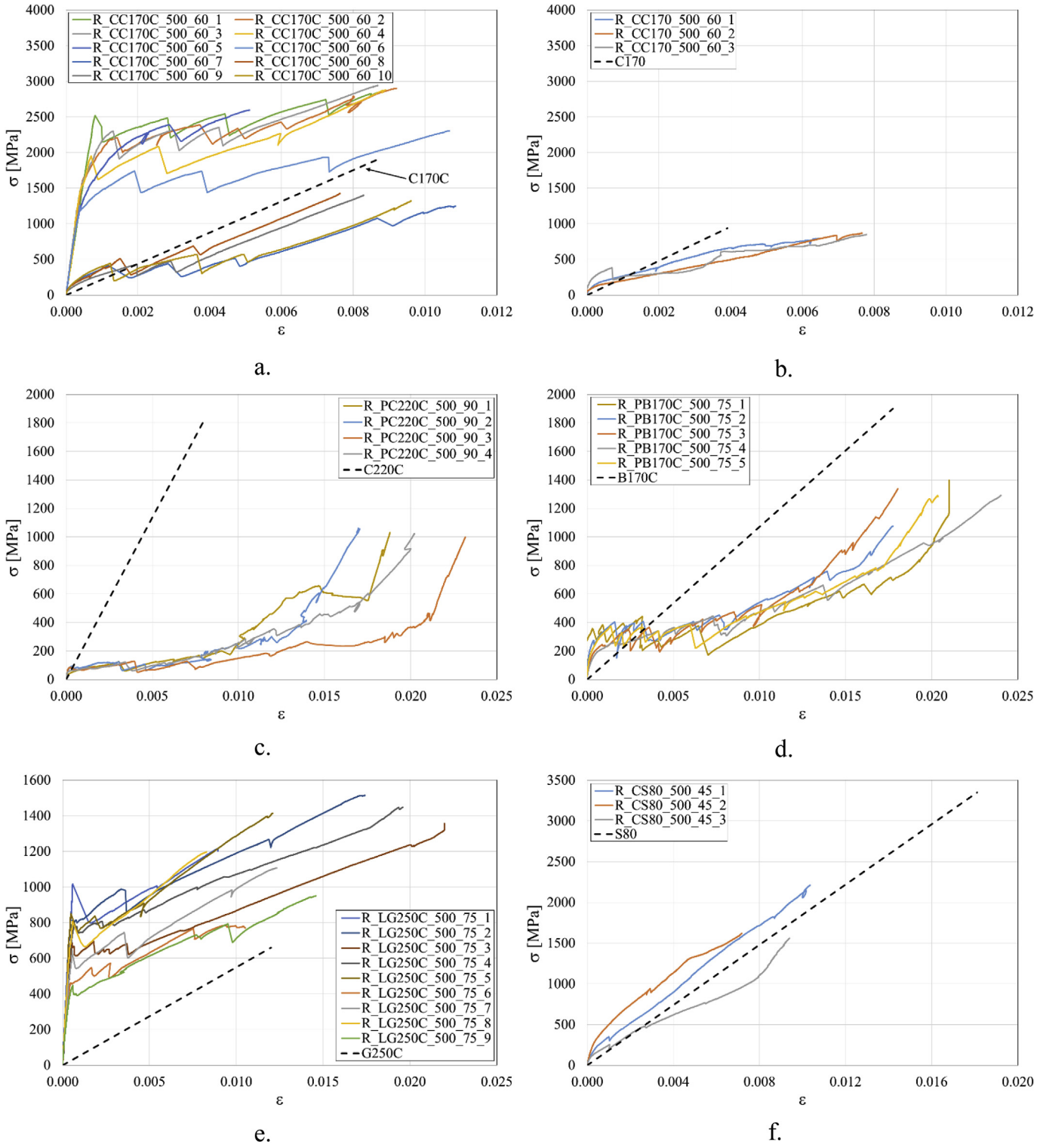

Fig. 4. Stress σ vs. strain ε of rectangular prism specimens of series a) R_CC170C_500_60, b) R_CC170_500_60, c) R_PC220C_500_90, d) R_PB170C_500_75, e) R_LG250C_500_75, and f) R_CS80_500_45. Note: dashed lines represent the response of single rovings.

area of the specimens and was indicated as $\sigma_{1,m}$ in Table 3. Although $\sigma_{1,m}$ is affected by the textile layout and by the set-up employed and should not be directly compared to the matrix tensile strength, it may provide an indication of the contribution of the matrix to Stage 1 and of the matrix-fiber composite behavior. All strain values were obtained as the average of the displacements measured by the two LVDTs over the corresponding base length (210 mm). FM in Table 3 indicates the failure mode observed and is given in a coded form explained in the next section. Finally, specimens of series R_CC170C_500_60 are subdivided into two sets due to the different behavior exhibited, as discussed in the next section.

4. Results and discussion

The obtained axial stress σ-axial strain ε curves are given in Fig. 4. For comparison, the stress-strain behavior of a single roving extracted from each textile (see Table 1) is also plotted in Fig. 4 with a dashed line.

It should be noted that matrix cracks often occurred both within and outside the base length of the LVDTs. Therefore, the strain measured is not always representative of the behavior of the entire specimen. However, consistency between results of specimens that reported matrix cracks outside the LVDTs base length and of specimens that reported matrix cracks only within the LVDTs base length suggests that the overall σ-ε behavior can be captured with the instrumentation and set-up employed in this study.

Three different failure modes were identified in tensile tests of TRM composites [24–28]: A) rupture of the fibers at a major crack near the clamping area (e.g. Fig. 5a); B) rupture of the fibers at a major crack far from the clamping area (e.g. Fig. 6); C) opening of a major crack close to the clamping area in combination with textile slippage within the matrix (e.g. Fig. 5b). Although mixed failure modes may occur, such as rupture of some fibers/yarns and sliding of some others, failure of each specimen was classified according to the prevalent mode of failure observed (see Table 3).

The location of a major crack that causes failure of the specimen should be random. When the clamping grip method is employed, however, stress concentrations induced by the clamping pressure may cause the opening of a major crack close to the clamping area. When the textile slips within the matrix after the opening of a major crack close to the clamping area (failure mode C) the composite tensile strength obtained should be lower than that obtained when the same composite fails due to fiber rupture (failure mode A and B). Therefore, for this type of test set-up (clamping grip) the composite tensile strength obtained from specimens failing under mode C should be disregarded.

When a major crack opens during a test, the fibers bridging that crack are loaded by the entire applied load and eventually fail provided that they are well-anchored from either side of the crack. The clamping pressure, which may be responsible of the occurrence of a major crack close to the clamping area, can adversely affect the fiber rupture stress. Depending on the magnitude of the clamping pressure, the triaxial state of stress on the fibers – which may result from the tensile load, clamping pressure, and matrix confinement close and within the clamping area – can lead to premature fiber rupture. Also, high levels of clamping pressure can locally damage the fibers, especially if cracks develop within the clamping area where the matrix is crushed against the textile.

Values of the 9 parameters obtained for rectangular prism specimens are reported in Table 3. When a crack development stage was not detectable, σ_2, ε_2, and E_2 could not be evaluated and are not reported in Table 3. Average (Avg) parameter values are reported in Table 3 together with the corresponding coefficients of variation (CoV). Series R_CC170C_500_60 was divided into two subseries (Table 3) because the behavior observed in Stage 1 of specimens of series R_CC170C_500_60_1-6 was noticeably different from that observed in specimens of series R_CC170C_500_60_7-10.

Parameters obtained from Stage 1 are quite scattered for all TRM composites tested. It should be noted that parameters of Stage 1 are mostly related to the matrix cross-sectional area and mechanical properties that are not directly taken into account by dividing the applied load by the area of the fibers.

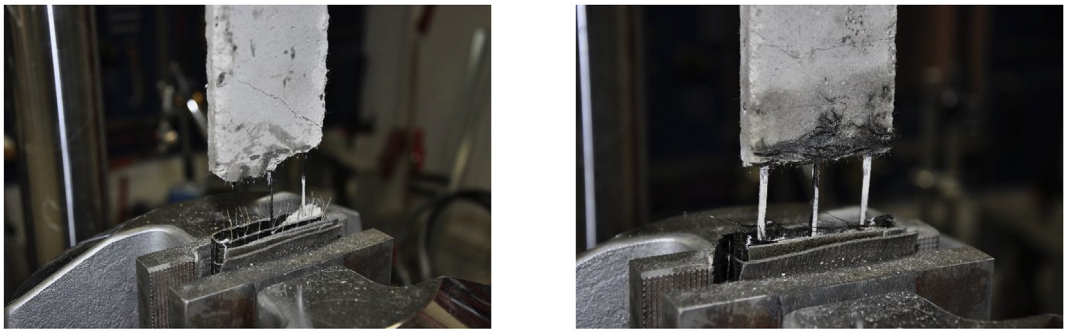

a. b.

Fig. 5. a) Failure mode A of specimen R_ CC170C_500_60_7. b). Failure mode C of specimen R_CC170C_500_60_8.

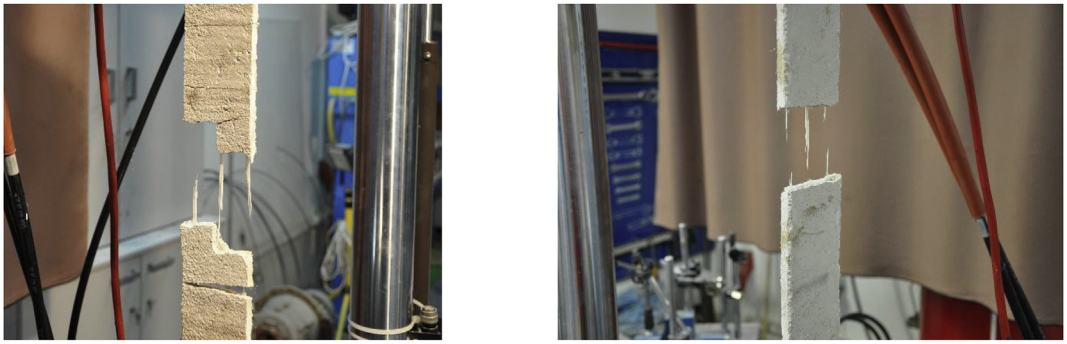

a. b.

Fig. 6. Failure mode B of specimen a) R_LG250C_500_75_3 and b) R_LG250C_500_75_8.

Parameters characterizing Stage 1 of specimens of series R_CC170C_500_60_7-10 are lower than those obtained from specimens of series R_CC170C_500_60_1-6. This behavior is attributed to pre-existing micro-cracking that might have had occurred during curing, handling, and setting-up of the spec-imens. This is confirmed by the very limited extent (almost zero) of the linear branch of Stage 1 for specimens of series R_CC170C_500_60_7-10 (Fig. 4a). It is interesting, though, that in terms of tensile strength the absence of Stage 1 entailed for a reduction of the maximum stress σ_u attained for specimens R_CC170C_500_60_7-10. This indicates that the presence of micro-cracks in the matrix did not allow for the redistribution of the applied load between the different bundles, leading to premature failure of the specimens. Although specimens R_CC170C_500_60_7-10 are characterized by stress values significantly lower than those of specimens R_CC170C_500_60_1-6, after Stage 1 stress-strain curves of the two series showed a similar behavior. Strain values corresponding to failure are comparable for all specimens with textile C170C, which suggests that the ultimate strain ε_u is not affected by the presence or absence of Stage 1 and by the stress level attained. Therefore, specimen failure was attributed to loss of bond between matrix and fibers and/or to gradual rupture of individual filaments, which were eventually damaged by friction (interlocking) with the matrix [14].

Stage 2 (where present) generally presented less scatter, although E_2 varied significantly for specimens of series R_LG250C_500_75. The ultimate stress σ_u obtained is consistent for each TRM composite tested except for specimens of series R_LG250C_500_75 and R_SS80_500_45. The ultimate strain ε_u varied from specimen to specimen because crack appeared outside the base length of the LVDTs affecting the results. The slope E_3 was consistent with the elastic modulus measured on single rovings extracted from each textile (Table 1) except for series R_CC170_500_60.

Specimens within each specimen series failed under the same failure mode, with exception of specimens R_CC170C_500_60_6 and 7, which failed under failure mode A whereas all specimens in each corresponding subseries failed under failure mode C, and specimen R_PB170C_500_75_4, which failed under failure mode B whereas all specimens in the same series failed under failure mode A. Specimens of series R_CC170C_500_60 that failed due to a major crack close to the clamping area in combination with textile slippage (failure mode C) reported an ultimate stress σ_u higher than the average ultimate stress of specimens in the same series that failed due to fiber rupture (failure mode A). This result is attributed to the uneven distribution of the applied load among different fiber bundles of specimens R_CC170C_500_60_6 and 7. Failure of these specimens, indeed, occurred due to fiber rupture at an inclined crack whereas failure of specimens in corresponding subseries occurred at a major crack orthogonal to the longitudinal fiber direction.

σ_u of specimen R_PB170C_500_75_4 is similar to that of other specimens in the same series. In this case the location of the major crack had no significant effect on the ultimate stress attained at fiber rupture, which indicates that the clamping pressure was not related to the rupture of fibers bridging the major crack close to the clamping area.

4.1. Effect of coating

Dry fiber rovings in TRM composites are generally not entirely impregnated because the matrix is not able to penetrate inside the yarn. This leads to a different behavior of the outer filaments of the yarn (firmly attached to the matrix) with respect to the (relatively free-to-slip) core filaments resulting in the well-documented telescopic behavior of the roving [44]. The stress-transfer mechanism of inner fiber filaments can be improved by the use of coating or, to a larger extent, of impregnation able to penetrate inside the yarn [38,42]. In addition, suitable sizing of fibers, which consists in the application of a film coat to each filament, is usually employed to protect the fibers and improve the adhesion with the matrix. When yarns are fully impregnated by resin, which is the case for all coated fiber textiles employed in this work, the stress-transfer capacity between inner and outer filaments is also enhanced.

In this study, the effect of fiber coating was investigated through tensile testing of two carbon textiles with the same area weight with (C170C) and without (C170) fiber coating. The presence of coating, which allowed for redistributing the load among the different filaments in each yarn, doubled the peak stress obtained from tensile tests on single rovings extracted from the textiles (see Table 1). It should be noted that each yarn of textile C170C comprised two coated fiber bundles twisted together. Failure of yarns of textile C170 occurred due to gradual rupture of individual filaments; complete yarn rupture was not observed until test termination (at 20% drop of maximum load attained – see Fig. 7a). Failure of yarns of textile C170C, on the other hand, occurred due to rupture of one of the two fiber bundles twisted together (Fig. 7b). Therefore, values of tensile strength measured for textiles C170C and C170 are strongly affected by the load redistribution between fiber bundles and between individual filaments within a single (and zero-twist) roving and represent a lower bound of the textile load-carrying capacity.

Rectangular prism specimens of TRM composites with textiles C170C and C170 and matrix type C were cast to investigate the effect of fiber coating. The results obtained from series R_CC170C_500_60_1-6, which are reported in Table 3, showed that the presence of fiber coating greatly improved the performance of the TRM composite leading to an ultimate stress approximately three times higher with respect to that obtained without coating (Fig. 4a and b). Stress σ_1 and slope E_1 are higher for specimens with coated fibers, which indicates a better matrix-fiber composite behavior for specimens R_CC170C_500_60_1-6 with respect to those of series R_CC170_500_60. In addition, the average of stress values $\sigma_{1,m}$ obtained from specimens R_CC170C_500_60_1-6 was higher than the estimated mean tensile strength of the plain cementitious mortar, f_{ctm}. f_{ctm} was calculated (for lack of a more appropriate formula) by the size-dependent relationship proposed by MC2010 [49] for concrete specimens, which provided a value of f_{ctm} equal to approximately half of the corresponding flexural strength (see results from flexural tests of matrix C prisms in Table 2). This indicates that the textile contributed to the load-carrying capacity also in Stage 1. Stage 2 of specimens with coated fibers is characterized by multiple cracks orthogonal to the specimen axis (a detail of a crack in specimen R_CC170C_500_60_5 is reported in Fig. 8a), which indicates good bond between matrix and fiber [29]. Stage 2 was absent for specimens with non-coated fibers; their behavior was characterized by the occurrence of a single crack corresponding to σ_1, which opened with increasing applied displacement (Fig. 8b). The single crack observed was not orthogonal to the axis of the specimens, which indicates that fiber yarns were not loaded in axial direction alone resulting in a lower load-carrying capacity in comparison to coated TRM specimens [29].

Specimens of series R_CC170C_500_60_1-6 reached a peak stress higher than the average tensile strength of a single fiber yarn extracted from the same textile used for the construction of the aforementioned specimens (Table 2 and dashed line in Fig. 4a). This difference is attributed to the presence of the inorganic matrix that allowed for uniform load redistribution both between bundles comprising each yarn and between different yarns.

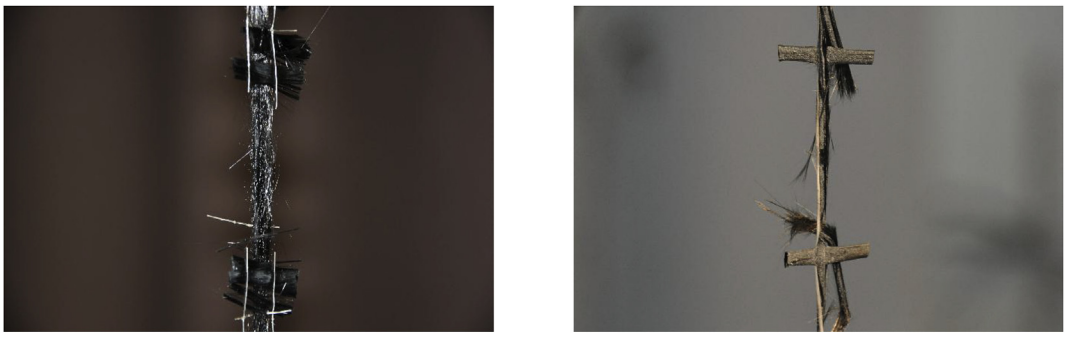

Fig. 7. Failure of single yarn of textiles a) C170 and b) C170C.

Fig. 8. Detail of a crack occurred in specimen a) R_CC170C_500_60_5 and b) R_CC170_500_60_3 (after completion of the test).

All specimens including matrix C and carbon fiber textiles (with and without coating) failed under mode C (Fig. 5a) except specimens R_CC170C_500_60_6 and 7 that failed under mode A (Fig. 5b). Although peak stress values of specimens R_CC170C_500_60_1-6 were significantly higher than those of single fiber yarns, the eventual slippage of the textile (failure mode C) indicates that the tensile capacity of the carbon fiber textile was not fully exploited.

A fiber coating was also applied to glass fiber textile G250C to protect the fibers against alkali attack and to improve the load distribution among the filaments. Coating of glass fiber bundles has been reported to highly improve the stress-strain response of dumbbell specimens subjected to tensile loading. Specimens comprising uncoated glass fiber textiles failed due to debonding and consequent slippage of the textile within the mortar whereas the use of coated glass fiber textiles allowed for attaining the tensile capacity of the fiber [50].

Stress-strain curves of specimens R_LG250C_500_75 (Fig. 4e) showed a trilinear behavior, although Stage 2 was not discernible for three specimens (Table 3). Failure occurred due to fiber rupture in all specimens (failure mode B - Fig. 6).

Values of stress σ_1 are scattered whereas the corresponding values of strain ε_1 are consistent between each other. Values of stress $\sigma_{1,m}$ obtained (as in the case of coated carbon TRMs) were slightly higher than the expected mean tensile strength of the plain mortar, f_{ctm} (assumed to be approximately half of its flexural strength [49] – see results from flexural tests of matrix L prisms in Table 2); this confirms that the coated textile contributes to the load uptake from the early stages of loading (Stage 1). Values of E_3 observed (average equal to 53 GPa) are consistent with the average elastic modulus measured on a single fiber yarn (E_f = 55 GPa, Table 2), which indicates that the clamping method adopted was effective and fibers were properly anchored between the grips. The peak stress reached by the TRM specimens is higher than the average tensile strength of a single fiber yarn (Table 2 and dashed line in Fig. 4e). Glass fiber yarns of textile G250C, similarly to carbon fiber yarns of textile C170C, comprised two fiber bundles twisted together. When tested under tension, single glass fiber yarns failed due to rupture of one of the intertwined fiber bundles providing a lower bound of the textile tensile strength. Furthermore, the presence of the matrix, as in the case of specimens R_CC170C_500_60_1-6, allowed for uniform load redistribution both between bundles comprising each yarn and between different yarns leading to a high degree of fiber exploitation (evidenced by fiber rupture) and, hence, to an increase of the maximum tensile stress attained (compared to the one corresponding to the single yarn).

4.2. Behavior of stitch-bonded textiles

In general, bidirectional textiles embedded in inorganic matrices consist of longitudinal and transversal bundles that are kept together through a secondary low-strength fiber net that provides a rather loose connection between orthogonal yarns. When such TRM composites are axially loaded the yarns normal to the direction of the applied load contribute to the load-carrying capacity of the composite only due to friction between them and the fiber yarns in the direction of the applied load. In order to increase the contribution of yarns normal to the applied load direction to the load-carrying capacity, warp and weft yarns can be stitch-bonded. In stitch-bonded (or otherwise firmly constructed, e.g. thermo-fixed) textiles, interlocking between yarns normal to the applied load direction and the matrix potentially increases the

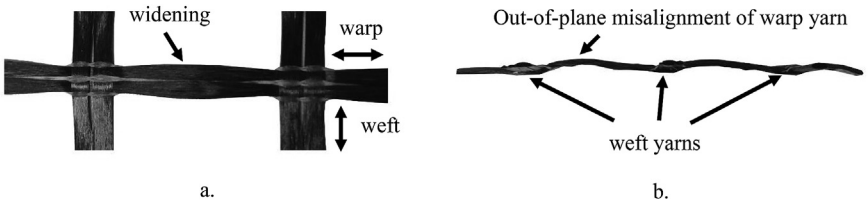

Fig. 9. Detail of a) widening of basalt B170C warp yarns between weft yarns and b) out-of-plane misalignment of carbon C220C warp yarns between weft yarns.

load-carrying capacity of the composite.

The behavior of the stitch-bonded carbon C220C and basalt B170C textiles embedded in the pozzolanic lime-based matrix P is studied in this paper. Textiles C220C and B170C are made using the conventional stitch-bonding process with the double tricot pattern, which provided a wavy shape of the warp rovings, whereas the weft rovings remained plane. With the conventional stitch-bonding process the knitting yarns fix the weft yarns only at crossing points with warp yarns. Therefore, the warp yarns are widened (Fig. 9a) and not perfectly aligned (Fig. 9b) between weft yarns [10]. This introduces a strain reserve in the warp yarns that has to be recovered before the yarns can carry the applied load.

When subjected to tensile loading, single warp yarns of textile C220C and B170C failed due to rupture of the whole yarn due to the presence of a fiber coating that allowed for uniform load redistribution between fiber filaments.

Results obtained from tensile tests on specimens of series R_PC220C_500_90 and R_PB170C_500_75 are shown in Fig. 4c and d, respectively. The stress-strain responses observed for carbon and basalt composites were similar. The matrix cracked at low levels of applied load providing small contribution to the load-carrying capacity of the specimens. Stress values $\sigma_{1,m}$ obtained for both carbon and basalt composites are low compared to the expected mean tensile strength of the plain mortar, f_{ctm} (assumed equal to approximately half of its flexural strength [49] – see results from flexural tests of matrix P prisms in Table 2). Low $\sigma_{1,m}$ values, which are associated to premature matrix cracking, can be explained in part by possible pre-existing micro-cracks in the matrix and, to a larger extent, by the presence of cross-sections where the matrix cross-sectional area is unsymmetrical and reduced due to offset of the textile from the mid-thickness plane and presence of stitch-bonded joints [10]. Basalt composites produced σ_1 values higher than those of carbon composites. This result is attributed to the different textile-to-matrix bond properties and to the different spacing between weft yarns of the two textiles. The shorter spacing between weft yarns of textile B170C (25 mm, see Table 1) than between weft yarns of textile C220C (30 mm, see Table 1) determines a higher degree of constraint to warp yarns in textiles B170C with respect to those in textile C220C. This constraint is in turn responsible for reducing the widening and misalignment (waviness) of the basalt warp yarns with respect to the carbon warp yarns. The waviness of carbon and basalt textiles is also responsible for the large extent of Stage 2, during which the textiles recovered the strain reserve caused by the waviness inducing numerous matrix cracks at a distance coinciding with the spacing of the weft yarns. Matrix cracks occurred right above weft yarns due to stress concentrations at the joints between warp and weft yarns and to the reduced thickness of the matrix in those areas [10]. In addition, the initial misalignment of the warp yarns, which is recovered with increasing applied displacement, caused spalling of the matrix (Fig. 10). With increasing applied displacement the warp yarns eventually recovered the initial misalignment and the stress-strain response passed on to Stage 3.

Different failure modes were observed for the two composites. Failure mode C was observed for specimens of series R_PC220C_500_90 and was attributed to two different reasons: (1) textile-to-mortar mechanical incompatibility (a "strong" textile + a "weak" mortar combination), and (2) insufficient pressure provided to the clamping grips (not enough to avoid fiber slippage and attain fiber failure). It should be noted that increasing the pressure applied to the clamping grips may prevent slippage of the textiles but it would require further strengthening of the specimen ends and/or increase of the gripped length to avoid matrix crushing in between wedges.

Failure mode A was observed for specimens of series R_PB170C_500_75 except for specimen R_PB170C_500_75_4 that failed under mode B. The slope of the stress-strain curves at Stage 3 was consistent with the elastic modulus of the single fiber yarns except for specimen R_PB170C_500_75_4, for which failure occurred due to progressive rupture of filaments (Fig. 10b).

It should be noted that specimens comprising basalt textile B170C and matrix P were also tested by other researchers [24] who applied a pretension force of 3 N per yarn during casting. By applying the pretension, the warp yarns misalignment was

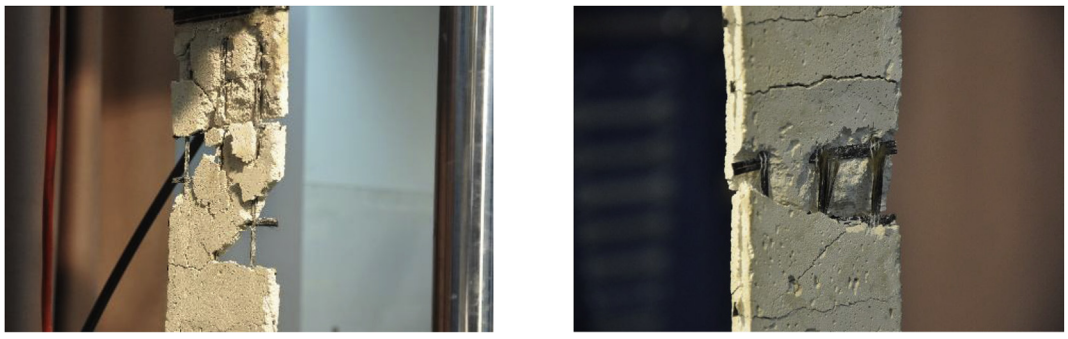

Fig. 10. a) Matrix spalling in specimen R_PC220C_500_90_3. b) Filaments rupture in specimens R_PB170C_500_75_4.

a. b.

Fig. 11. a) Opening of a major crack close to the grips at the end of test in specimen R_CS80_500_45_2. b) Crack pattern of specimen R_CS80_500_45_3.

recovered, matrix spalling was avoided and stress values obtained were generally higher than those reported for series R_PB170C_500_75 for a given strain ε.

4.3. Composites with steel cords

Results obtained from prismatic coupons of rectangular cross-section consisting of steel cords S80 (one layer) embedded in matrix type C (series R_CS80_500_45) are shown in Fig. 4f. All specimens tested failed due to the sudden opening of a major crack close to the clamping area associated with slippage of the steel cords within the matrix (failure mode C). Slippage of cords within the matrix, which was also observed by other researchers for different inorganic-matrix composites with steel cords [27], is again attributed to both textile-to-mortar mechanical incompatibility (a 'strong' textile + a 'weak' mortar combination) and insufficient clamping force applied (approximately 76 kN) which was not enough to avoid textile slippage and attain cords rupture. However, E_3 values obtained (Table 3) are consistent with the elastic modulus measured from tensile tests on individual cords, $E_f = 185$ GPa (Table 1 and dashed line in Fig. 4f), which suggests that the clamping method employed allowed for characterizing the composite material until mode C failure occurred. The σ-ε curves obtained are characterized by a limited Stage 1 and by the absence of a clearly detectable Stage 2. The cracking strain ε_1 was computed as the strain corresponding to the point of intersection between lines with slope E_1 and E_3 (see Fig. 1b), whereas σ_1 was obtained as the stress corresponding to ε_1 on the σ-ε curve. Although multiple matrix cracks occurred along the specimens (Fig. 11), drops in the applied stress were not observed suggesting that the matrix did not provide a significant contribution to the load-carrying capacity after Stage 1. Values of $\sigma_{1,m}$ obtained (Table 3) were particularly low with respect to the (estimated) tensile strength of the plain mortar [49]. The clamping force applied (approximately 76 kN) resulted in a clamping stress of approximately 21.10 MPa, which is higher than the compressive strength of the matrix employed ($\sigma_c = 16.40$ MPa, see Table 2). Although the presence of FRP wraps at the specimen ends may have increased the compressive strength of the matrix by limiting transversal strains, the high clamping stress may have caused cracking of the matrix between the wedges, which in turn may have led to the reduced matrix contribution to the applied load (i.e. low values of σ_1 and $\sigma_{1,m}$) and may have promoted slippage of the cords. It should be noted that wrapping of specimen ends does not allow to verify whether the matrix is cracked between the wedges.

5. Conclusions

The tensile behavior of six different composite materials comprising high strength fiber textiles embedded in inorganic matrices is studied in this paper. Fiber textiles consisted of carbon, glass, basalt, or steel fibers and were embedded in cement- or lime-based matrices. The influence of textile coating on the stress-strain response was investigated. In addition, the behavior of stitch-bonded textiles was critically assessed. The results obtained from 32 rectangular prism specimens tested using the clamping grip method allowed for drawing the following conclusions:

- The use of the clamping grip method did not always allow for obtaining textile rupture far from the clamping areas (failure mode B). Although some specimens failed due to fiber rupture near the clamping area (failure mode A) or fiber slippage within the matrix (failure mode C), textiles started to slip only after the opening of a major crack, which allowed the passing on to Stage 3 for all composite materials. Increasing the pressure applied to the clamping grips may prevent slippage of textiles but would imply further strengthening of specimen ends and/or increasing of the gripped length to avoid matrix crushing between wedges.

- Test results on rectangular prism specimens were affected by curing, handling, and setting-up of specimens that may have caused micro-cracking in the matrix. Pre-existing micro-cracking in the matrix affects not only parameters of Stage 1 but the entire stress-strain response leading to premature failure of the specimens.
- For specimens comprising coated glass fiber textile G250C and coated carbon fiber textile C170C the load redistribution provided by the matrix led to peak stresses higher than the tensile strengths obtained from single yarns (in the direction of loading) extracted from corresponding textiles comprising the composites.
- The idealized trilinear stress-strain behavior was not observed in all specimens. The evaluation of parameters characterizing the stress-strain behavior was not an easy task. Although values of ultimate stress were consistent between specimens of the same TRM composite, results obtained for the remaining parameters were generally scattered.
- The use of coatings that fully impregnated the textile yarns allowed for uniform load redistribution between fiber filaments and between fiber bundles, which resulted in a considerable improvement of the mechanical characteristics of the carbon composite with coated textile with respect to that with uncoated textile.
- Stitch-bonded textiles, which presented misalignment and widening of warp yarns, led to matrix spalling in tensile tests of rectangular prism specimens. Misalignment (waviness) and widening of warp yarns determined the large extent of Stage 2, during which the textiles recovered the strain reserve inducing numerous matrix cracks at a distance coinciding with the spacing of the weft yarns.

Acknowledgements

The work discussed in this paper was conducted within the framework of Endure-ITN under grant no. 607851. Parts of the analysis were developed within the activities of the RRT campaign organized by Rilem TC 250-CSM. Fyfe Europe S.A. (Greece) and G&P Intech s.r.l. Altavilla Vicentina (Italy) are gratefully acknowledged for providing the composite materials. The authors also express their gratitude to Mr. Panagiotis Rompakis for helping during the experimental campaign.

References

[1] Buyukozturk O, Gunes O, Karaca E. Progress on understanding debonding problems in reinforced concrete and steel members strengthened using FRP composites. Constr Build Mater 2004;18(1):9–19.
[2] Colombo I, Colombo M, Magri A, Zani G, di Prisco M. Textile reinforced mortar at high temperatures. In Appl Mech Mater 2011;82:202–7.
[3] Bisby L, Stratford T, Hart C, Farren S. Fire Performance of well-anchored TRM, FRCM, and FRP flexural strengthening systems. Belfast, UK: Network Group for Composites in Construction; 2013. Adv Compos in Constr.
[4] Tetta ZC, Bournas DA. TRM vs. FRP jacketing in shear strengthening of concrete members subjected to high temperatures. Compos Part B Eng 2016;106:190–205.
[5] Sneed LH, D'Antino T, Carloni C. Investigation of bond behavior of PBO fiber-reinforced cementitious matrix composite-concrete interface. ACI Mater J 2014;111(5):569–80.
[6] Triantafillou TC, Papanicolaou CG. November. Textile reinforced mortars (TRM) versus fiber reinforced polymers (FRP) as strengthening materials of concrete structures. In: Proceedings of the 7th ACI international symposium on fibre-reinforced (FRP) polymer Reinforcement for concrete structures. American Concrete Institute; 2005. p. 99–118.
[7] De Felice G, De Santis S, Garmendia L, Ghiassi B, Larrinaga P, Lourenco PB, et al. Mortar-based systems for externally bonded strengthening of masonry. Mater Struct 2014;47:2021–37.
[8] Mobasher B, Peled A, Pahilajani J. Distributed cracking and stiffness degradation in fabric-cement composites. Mater Struct 2006;39(3):317–31.
[9] Jesse F, Schicktanz K, Curbach M. Obtaining characteristic material strength of Textile Reinforced Concrete (TRC) from laboratory tests. In: Proceedings of 9th international symposium on ferrocement (Ferro9); May 18-20, 2009. p. 305–18. Bali.
[10] Hausding J, Lorenz E, Ortlepp R, Lundahl A, Cherif C. Application of stitch-bonded multi-plies made by using the extended warp knitting process: reinforcements with symmetrical layer arrangement for concrete. J Text Inst 2011:1–13. http://dx.doi.org/10.1080/00405000.2010.515729.
[11] Triantafillou TC. Textile-reinforced mortars (TRM) versus fibre-reinforced polymers (FRP) as strengthening and seismic retrofitting materials for reinforced concrete and masonry structures. In: Int. Conf. On advanced composites in construction (ACIC07); 2007, April.
[12] ACI Committee. 549, ACI 549.4R-13 – guide to Design and construction of externally bonded fabric-reinforced cementitious matrix (FRCM) systems for repair and strengthening concrete and masonry structures. 2013.
[13] Bisby LA, Stratford TJ, Roy EC, Ward M. Fibre reinforced cementitious matrix systems for fire-safe flexural strengthening of concrete: pilot testing at ambient temperatures. In: Proceedings of advanced composites in construction conference (ACIC). NetComposites Ltd; 2009. p. 449–60.
[14] D'Ambrisi A, Focacci F. Flexural strengthening of RC beams with cement-based composites. J Compos Constr 2011;15(5):707–20.
[15] D'Antino T, Carloni C, Sneed LH, Pellegrino C. Matrix-fiber bond behavior in PBO FRCM composites: a fracture mechanics approach. Eng Frac Mech 2014;117:94–111.
[16] Carozzi FG, Poggi C. Mechanical properties and debonding strength of fabric reinforced cementitious matrix (FRCM) systems for masonry strengthening. Compos Part B Eng 2015;70:215–30. http://dx.doi.org/10.1016/j.compositesb.2014.10.056.
[17] Arboleda D, Carozzi FG, Nanni A, Poggi C. Testing procedure for the uniaxial tensile characterization of fabric-reinforced cementitious matrix composites. J Compos Constr 2015. http://dx.doi.org/10.1061/(ASCE)CC.1943-5614.0000626.
[18] De Santis S, de Felice G. Steel reinforced grout systems for strengthening of masonry structures. Comp Struct 2015;134:533–48.
[19] D'Ambrisi A, Focacci F, Luciano R, Alecci V, De Stefano M. Carbon-FRCM materials for structural upgrade of masonry arch road bridges. Compos Part B Eng 2015;75:355–66. http://dx.doi.org/10.1016/j.compositesb.2015.01.024.
[20] AC434. Acceptance criteria for masonry and concrete strengthening using fiber-reinforced cementitious matrix (FRCM) composite systems. Whittier, CA: ICC-Evaluation Service; 2013.
[21] IBC I. International code Council. International building code. Washington DC, United States: International Code Council; 2012.
[22] Carloni C, Bournas DA, Carozzi FG, D'Antino T, Fava G, Focacci F, et al. Fiber reinforced composites with cementitious (inorganic) matrix. Chapter 9. 349e391. In: Pellegrino C, Sena-Cruz J, editors. Design procedures for the use of composites in strengthening of reinforced concrete structures e state of the art report of the RILEM TC 234-DUC, vols. Springer; 2015. p. 501 [RILEM STAR Book Series].
[23] RILEM Technical Committee 232-TDT (Wolfgang Brameshuber). Recommendation of RILEM TC 232-TDT: test methods and design of textile reinforced concrete - uniaxial tensile test: test method to determine the load bearing behavior of tensile specimens made of textile reinforced concrete. Mater Struct 2016. http://dx.doi.org/10.1617/s11527-016-0839-z.
[24] Lignola GP, Caggegi C, Ceroni F, De Santis S, Krajewski P, Lourenco P, et al. Performance assessment of Basalt FRCM for retrofit applications on masonry. Compos Part B: Eng, http://dx.doi.org/10.1016/j.compositesb.2017.05.003.
[25] Carozzi FG, Bellini A, D'Antino T, de Felice G, Focacci F, Hojdys L, et al. Experimental investigation of tensile and bond properties of Carbon-FRCM composites for strengthening masonry elements. Compos Part B Eng, http://dx.doi.org/10.1016/j.compositesb.2017.06.018.
[26] Leone M, Aiello MA, Balsamo A, Carozzi FG, Ceroni F, Corradi M, et al. Glass fabric reinforced cementitious matrix: tensile properties and bond performance on masonry substrate. Compos Part B Eng, http://dx.doi.org/10.1016/j.compositesb.2017.06.028.
[27] De Santis S, Ceroni F, de Felice G, Fagone M, Ghiassi B, Kwiecien A, et al. Round Robin test on tensile and bond behavior of steel reinforced grout systems. Compos Part B Eng, http://dx.doi.org/10.1016/j.compositesb.2017.03.052.
[28] Caggegi C, Carozzi FG, De Santis S, Fabbrocino F, Focacci F, Hojdys L, et al. Experimental analysis on tensile and bond properties of PBO and Aramid fabric reinforced cementitious matrix for strengthening masonry structures. Compos Part B Eng, http://dx.doi.org/10.1016/j.compositesb.2017.05.048.
[29] Hegger J, Will N, Bruckermann O, Voss S. Load-bearing behavior and simulation of textile reinforced concrete. Mater Struct 2006;39:765–76. http://dx.doi.org/10.1617/s11527-005-9039-y.
[30] Ascione L, de Felice G, De Santis S. A qualification method for externally bonded fibre reinforced cementitious matrix (FRCM) strengthening systems. Compos Part B Eng 2015;78:497–506. DOI: 1016/j.compositesb.2015.03.079.
[31] Contamine R, Si Larbi A, Hamelin P. Contribution to direct tensile testing of textile reinforced concrete (TRC) composites. Mater Sci Eng A 2011;528:8589–98. http://dx.doi.org/10.1016/j.msea.2011.08.009.
[32] Brockmann J, Raupach M. Durability investigations on textile reinforced concrete. Durability of Materials and Components. Brisbane, Australia. In: 9th international conference (CSIRO 2002); March 2002. p. 17–20. Paper No. 111.
[33] Orlowsky J, Raupach M. Modeling the loss in strength of AR-glass fibers in textile-reinforced concrete. Mater Struct 2006;39:635–43. http://dx.doi.org/10.1617/s11527-006-9100-5.
[34] Papantoniou IC, Papanicolaou CG. Flexural behavior of one-way textile

reinforced concrete (TRC)/reinforced concrete (RC) composite slabs. Venice, Italy. In: Proceedings of the 15th european conference on composite materials - ECCM15; 2012. p. 24–8. June 2012 (in CD Proceedings).
[35] Pellegrino C, D'Antino T. Experimental behavior of existing precast prestressed reinforced concrete elements strengthened with cementitious composites. Compos Part B Eng 2013;55:31–40.
[36] Donnini J, Corinaldesi V, Nanni A. Mechanical properties of FRCM using carbon fabrics with different coating treatments. Compos Part B Eng 2016;38:220–8. http://dx.doi.org/10.1016/j.compositesb.2015.11.012.
[37] Dugas M, Weise S, Curbach M, Hempel R, Offermann P, Franzke G. Force-deformation behaviour of tensileloaded specimens made of Textile Reinforced Concrete. In: Techtextil symposium 1998; 1998. p. 143–52. Lyon.
[38] Hartig J, Jesse F, Schicktanz K, Haußler-Combe U. Influence of experimental setups on the apparent uniaxial tensile load-bearing capacity of textile-reinforced concrete specimens. Mater Struct 2012;45:433–46. http://dx.doi.org/10.1617/s11527-011-9775-0.
[39] Carloni C, Verre S, Sneed LH, Ombres L. Loading rate effect on the debonding phenomenon in fiber reinforced cementitious matrix-concrete joints. Compos Part B Eng 2017;108:301–14.
[40] Loreto G, Leardini L, Arboleda D, Nanni A. Performance of RC slab-type elements strengthened with fabric-reinforced cementitious-matrix composites. J Compos Constr 2013;18(3):1–9.
[41] Raoof S, Koutas L, Bournas DA. Bond between textile-reinforced mortar (TRM) and concrete substrates: experimental investigation. Compos Part B Eng 2016;98:350–61.
[42] Hegger J, Will N, Curbach M, Jesse F. Tragverhalten von Textilbewehrtem Beton (Load-Bearing behaviour of TRC) Beton- und Stahlbetonbau 99, vol. 6; 2004. p. 452–5.
[43] Jesse F, Will N, Curbach M, Hegger J. Load-bearing behavior of textile-reinforced concrete, 250. Special Publicationvol.; 2008. p. 59–68.
[44] Banholzer B. Bond behavior of multi-filament yarn embedded in a cementitious matrix. PhD Thesis. United Kingdom: RETH Aachen University; 2004.
[45] Li VC. Engineered cementitious composites (ECC) – material, structural, and durability performance. In: Nawy, editor. Concrete construction engineering handbook, chapter 24. CRC Press; 2008.
[46] Brameshuber W. Report 36: textile reinforced concrete-state-of-the-art report of RILEM TC 201-TRC, vol. 36. RILEM publications; 2006.
[47] ASTM. Standard test method for tensile properties of polymer matrix composite materials. D3039/D3039M, ASTM International. 1996. p. 6.
[48] Comité Européen De Normalization. Methods of test for mortar for masonry – Part 11: determination of flexural and compressive strength of hardened mortar. UNI EN. Brussels, Belgium. 2007. 12 pages.
[49] FIB (Federation Internationale du Beton). Fib model code for concrete structures 2010. October 2013. p. 434. ISBN: 978-3-433-03061-5.
[50] Lyras I. Experimental investigation of the mechanical behavior of textile reinforced cementitious mortars under tension. M.Sc. Thesis. Civil Engineering Department, University of Patras (in Greek); 2010.